PERGAMON

International Journal of Solids and Structures 39 (2002) 4979–4998

INTERNATIONAL JOURNAL OF SOLIDS and STRUCTURES

www.elsevier.com/locate/ijsolstr

Saint-Venant end effects in multilayered piezoelectric laminates

Jiann-Quo Tarn [a,*], Li-Jeng Huang [b]

[a] *Department of Civil Engineering, National Cheng Kung University, Tainan 70101, Taiwan*
[b] *Department of Civil Engineering, National Kaohsiung University of Applied Science Kaohsiung 80701, Taiwan*

Received 26 September 2001; received in revised form 2 July 2002

Abstract

The Saint-Venant end effects and stress decay in multilayered laminates of piezoelectric materials are studied. A state space approach is developed in the context of generalized plane strain. By means of matrix algebra and transfer matrix, the characteristics of the stress decay in 2-D piezoelectric strips and laminates are examined. Their elastic counterparts are included as special cases. Evaluation of the characteristic decay length for typical materials shows that the Saint-Venant end effects are significant. It also indicates that the analysis based on the plane strain assumption is misleading.

Keywords: Saint-Venant's principle; Piezoelectric laminates; End effects; Generalized plane strain; Stress decay

1. Introduction

Due to increasing use of piezoelectric ceramics and polymers, mechanics of piezoelectric materials has attracted considerable attention. The problem of stress decay in an anisotropic piezoelectric material, known as the Saint-Venant end effect, is of fundamental importance in strain measurement. An understanding of the characteristics of stress decay is useful in the design of sensors and piezoelectric specimens. When a piezoelectric body is subjected to electromechanical loading, the electric and mechanical fields interact. Because of electromechanical interaction and combined effects of anisotropy and lamination, electroelastic analysis of a piezoelectric laminate is much more involved than its elastic counterpart. A great amount of work concerning the response of laminated structures with piezoelectric layers has been published (see, for example, the review articles by Saravanos and Heyliger, 1999; Gopinathan et al., 2000 and the references therein). In dealing with stress decay in laminates, numerical techniques such as the displacement-based finite element method are not very useful because the field variables vary drastically near the ends. In order to develop a computational model the nature of the decay must be captured analytically. Although the stress decay in an anisotropic elastic material has been under extensive study (see Horgan and

* Corresponding author. Fax: +886-6-2358542.
E-mail address: jqtarn@mail.ncku.edu.tw (J.-Q. Tarn).

0020-7683/02/$ - see front matter
PII: S0020-7683(02)00424-9

Knowles, 1983; Horgan, 1989, 1996; Ting, 1996, and the references therein), few analyses in the case of a piezoelectric material have been reported. Among them, Batra and Yang (1995) extended Saint-Venant's principle of elasticity (Toupin, 1965) to linear piezoelectricity and showed that the energy stored in the portion of a prismatic bar beyond a distance s from the loaded end decreases *exponentially* with the distance s. Ruan et al. (2000) employed the stress function approach to investigate the Saint-Venant end effects in a 2-D semi-infinite piezoceramic strip. In order to simplify the analysis, they ignored the antiplane field variables outright and assumed that the gradient of the electric potential is smaller in the axial direction than in the thickness direction. It is known that the stress function approach is ineffective in treating a multilayered system (Wang et al., 2000; Tarn and Wang, 2001). Moreover, analysis of piezoelectric strips based on plane strain or plane stress assumption is questionable.

In this paper we develop a state space approach for the Saint-Venant end effects in piezoelectric laminates in the context of generalized plane strain (Lekhnitskii, 1981; Ting, 1996). The piezoelectric material considered belongs to the *monoclinic system of class 2* (Nye, 1957) of which the *orthorhombic* system is a special case. Stress singularity is known to occur at the free edges of a laminate. Herein the stress decay away from the edges is of primary concern. Investigation of the free-edge singularity is beyond the scope of the present study. When the laminate strip is subjected to self-equilibrated loads at the ends, the stress and strain are independent of the longitudinal coordinate x_2, but the displacements depend on x_2 and all the field variables—antiplane as well as inplane—enter the picture. In a state space formulation the field variables are not eliminated, rather, the primary state variables are identified and the field equations are cast into a state equation. For a piezoelectric laminate the primary state variables are the displacements, transverse stresses, electric potential and electric displacement in the thickness direction because the interfacial continuity and boundary conditions are directly associated with them (Tarn, 2001, 2002a,b). Guided by previous studies for an elastic material (Horgan, 1989, 1996; Ting, 1996; Wang et al., 2000) and the theoretical basis by Batra and Yang (1995), we seek an eigensolution in the form of exponential decay functions of the distance from the ends. The smallest decay factor is a measure of the characteristic decay length and the attenuation rate of the end effects. The characters of the stress decay are reflected through the eigenvalues and eigenmodes of the problem. In determining the eigensolution for a piezoelectric laminate, the transfer matrix is employed to satisfy the interfacial continuity and boundary conditions. The advantage is that it requires only a systematic operation of 8×8 matrices, regardless of the number of layers. To understand the characteristics of the end effects, the self-equilibrated fields and decay lengths in 2-D homogeneous piezoelectric strips and laminates with integrated piezoelectric layers are evaluated for typical piezoelectric materials. The results show that the Saint-Venant end effects are significant and decay length far-reaching. Mixed modes occur in general; only for a special class of the orthorhombic piezoelectric material do the inplane and antiplane fields uncouple. More importantly, plane strain or plane stress assumption is invalid even when the piezoelectric strip is subjected to 2-D electromechanical loading. Antiplane field variables must not be neglected in the formulation. The results obtained herein are useful in developing a numerical model for versatile computation.

2. State space formulation

Consider a piezoelectric laminate composed of n layers in a self-equilibrated state (Fig. 1). The piezoelectric material belongs to *monoclinic system of class 2* with the x_3-axis being the polarization direction (Nye, 1957). The constitutive equations of the material are

$$\begin{bmatrix} \boldsymbol{\varepsilon} \\ \mathbf{D} \end{bmatrix}_k = \begin{bmatrix} \mathbf{S} & \mathbf{d} \\ \mathbf{d}^{\mathrm{T}} & \boldsymbol{\kappa} \end{bmatrix}_k \begin{bmatrix} \boldsymbol{\sigma} \\ \boldsymbol{\Phi} \end{bmatrix}_k, \tag{1}$$

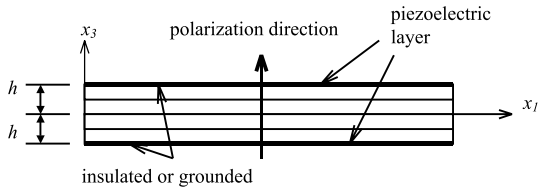

Fig. 1. Schematic of a piezoelectric laminate.

where

$$\boldsymbol{\varepsilon} = [\,\varepsilon_{11} \quad \varepsilon_{22} \quad \varepsilon_{33} \quad 2\varepsilon_{23} \quad 2\varepsilon_{13} \quad 2\varepsilon_{12}\,]^{\mathrm{T}}, \quad \mathbf{D} = [\,D_1 \quad D_2 \quad D_3\,]^{\mathrm{T}},$$

$$\boldsymbol{\sigma} = [\,\sigma_{11} \quad \sigma_{22} \quad \sigma_{33} \quad \sigma_{23} \quad \sigma_{13} \quad \sigma_{12}\,]^{\mathrm{T}}, \quad \boldsymbol{\Phi} = -[\,\phi_{,1} \quad \phi_{,2} \quad \phi_{,3}\,]^{\mathrm{T}},$$

ε_{ij} and σ_{ij} are the strain and stress tensors, ϕ is the electric potential, D_i is the electric displacement vector. The explicit expression of the material matrices $\mathbf{S}$, $\mathbf{d}$ and $\boldsymbol{\kappa}$ are given in Appendix A, in which s_{ij} are the 13 elastic compliances measured at a constant electric field, κ_{ij} the permittivity constants measured at constant stress, d_{ij} the coefficients of the converse piezoelectric effect. The comma denotes the partial differentiation with respect to the suffix variables. The subscript k denotes the kth layer, k runs from 1 to n.

Eq. (1) is the constitutive equations for various classes of piezoelectric materials, including among others, the *orthorhombic* system of class *mm*2 by setting $s_{16} = s_{26} = s_{36} = s_{45} = d_{14} = d_{25} = d_{36} = \kappa_{12} = 0$, and those of class 6*mm* by setting, additionally, $s_{11} = s_{22}$, $s_{13} = s_{23}$, $s_{44} = s_{55}$, $s_{66} = 2(s_{11} - s_{12})$, $d_{15} = d_{24}$, $d_{31} = d_{32}$, $\kappa_{11} = \kappa_{22}$. The equations of elasticity are coupled to the equations of electrostatics through d_{ij} (Tiersten, 1969). The constitutive equations of a *monoclinic anisotropic elastic* material, having one plane of symmetry parallel to the planes $x_3 =$ constant, are a special case of Eq. (1) with $d_{ij} = 0$.

The strain–displacement relations are

$$\varepsilon_{ij} = (u_{i,j} + u_{j,i})/2. \tag{2}$$

The equations of equilibrium in the absence of body forces are

$$\sigma_{ij,j} = 0. \tag{3}$$

The equations of electrostatics without free charges are

$$D_{i,i} = 0. \tag{4}$$

For the problem under study the laminate is subjected to self-equilibrated loads at $x_1 = 0$ and a (Fig. 1). The top and bottom surfaces are free from traction and electric voltage or charge such that

$$\sigma_{13} = \sigma_{23} = \sigma_{33} = 0, \quad \text{and } \phi = 0 \text{ or } D_3 = 0 \quad \text{on } x_3 = \pm h, \tag{5}$$

where $\phi = 0$ on a grounded surface, $D_3 = 0$ on an electric-insulated surface.

The continuity conditions on the interface $x_3 = z_k$, $(k = 1, 2, \ldots, n-1)$ require

$$[\,u_1 \quad u_2 \quad u_3 \quad \phi\,]_k = [\,u_1 \quad u_2 \quad u_3 \quad \phi\,]_{k+1}, \tag{6}$$

$$[\,\sigma_{13} \quad \sigma_{23} \quad \sigma_{33} \quad D_3\,]_k = [\,\sigma_{13} \quad \sigma_{23} \quad \sigma_{33} \quad D_3\,]_{k+1}. \tag{7}$$

In order to make the formulation concise, we separate the field variables into the transverse components and those in the x_1–x_2 plane (denoted by a subscript p), and rewrite Eq. (1) as

$$\boldsymbol{\varepsilon}_p = \mathbf{S}_{pp}\boldsymbol{\sigma}_p + \mathbf{S}_{p3}\sigma_{33} - \mathbf{d}_p\phi_{,3}, \tag{8}$$

$$\varepsilon_{33} = \mathbf{S}_{p3}^{\mathrm{T}}\boldsymbol{\sigma}_p + s_{33}\sigma_{33} - d_{33}\phi_{,3}, \tag{9}$$

$$\boldsymbol{\varepsilon}_s = \mathbf{S}_{ss}\boldsymbol{\sigma}_s - \mathbf{d}_s\mathbf{L}\phi, \tag{10}$$

$$\mathbf{D}_p = \mathbf{d}_s^{\mathrm{T}}\boldsymbol{\sigma}_s - \boldsymbol{\kappa}\mathbf{L}\phi, \tag{11}$$

$$D_3 = \mathbf{d}_p^{\mathrm{T}}\boldsymbol{\sigma}_p + d_{33}\sigma_{33} - \kappa_{33}\phi_{,3}, \tag{12}$$

where

$$\boldsymbol{\varepsilon}_p = [\,\varepsilon_{11} \quad \varepsilon_{22} \quad 2\varepsilon_{12}\,]^{\mathrm{T}}, \quad \boldsymbol{\sigma}_p = [\,\sigma_{11} \quad \sigma_{22} \quad \sigma_{12}\,]^{\mathrm{T}},$$

$$\boldsymbol{\varepsilon}_s = [\,2\varepsilon_{13} \quad 2\varepsilon_{23}\,]^{\mathrm{T}}, \quad \boldsymbol{\sigma}_s = [\,\sigma_{13} \quad \sigma_{23}\,]^{\mathrm{T}}, \quad \mathbf{D}_p = [\,D_1 \quad D_2\,]^{\mathrm{T}},$$

$$\mathbf{S}_{pp} = \begin{bmatrix} s_{11} & s_{12} & s_{16} \\ s_{12} & s_{22} & s_{26} \\ s_{16} & s_{26} & s_{66} \end{bmatrix}, \quad \mathbf{S}_{p3} = \begin{bmatrix} s_{13} \\ s_{23} \\ s_{36} \end{bmatrix}, \quad \mathbf{d}_p = \begin{bmatrix} d_{31} \\ d_{32} \\ d_{36} \end{bmatrix},$$

$$\mathbf{S}_{ss} = \begin{bmatrix} s_{55} & s_{45} \\ s_{45} & s_{44} \end{bmatrix}, \quad \mathbf{d}_s = \begin{bmatrix} d_{15} & d_{25} \\ d_{14} & d_{24} \end{bmatrix}, \quad \boldsymbol{\kappa} = \begin{bmatrix} \kappa_{11} & \kappa_{12} \\ \kappa_{12} & \kappa_{22} \end{bmatrix}, \quad \mathbf{L} = \begin{bmatrix} \partial/\partial x_1 \\ \partial/\partial x_2 \end{bmatrix}.$$

In the formulation u_1, u_2, u_3, ϕ, $\boldsymbol{\sigma}_s$, σ_{33} and D_3 are taken to be the primary state variables and $\boldsymbol{\sigma}_p$ and $\mathbf{D}_p$ are expressed in terms of them. To this end, we arrange the basic equations into

$$\mathbf{u}_{,3} = -\mathbf{L}u_3 - \mathbf{d}_s\mathbf{L}\phi + \mathbf{S}_{ss}\boldsymbol{\sigma}_s, \tag{13}$$

$$u_{3,3} = \widetilde{\mathbf{S}}_{p3}^{\mathrm{T}}\mathbf{S}_{pp}^{-1}\mathbf{L}_p\mathbf{u} + (\widetilde{s}_{33} - \mathbf{S}_{p3}^{\mathrm{T}}\mathbf{S}_{pp}^{-1}\widetilde{\mathbf{S}}_{p3})\sigma_{33} + \widetilde{d}_{33}D_3, \tag{14}$$

$$\phi_{,3} = \widetilde{\kappa}_{33}^{-1}\mathbf{d}_p^{\mathrm{T}}\mathbf{S}_{pp}^{-1}\mathbf{L}_p\mathbf{u} + \widetilde{d}_{33}\sigma_{33} - \widetilde{\kappa}_{33}^{-1}D_3, \tag{15}$$

$$\boldsymbol{\sigma}_{s,3} = -\mathbf{L}_p^{\mathrm{T}}[\mathbf{S}_{pp}^{-1}(\mathbf{G}\mathbf{L}_p\mathbf{u} - \widetilde{\mathbf{S}}_{p3}\sigma_{33} - \widetilde{\kappa}_{33}^{-1}\mathbf{d}_pD_3)], \tag{16}$$

$$\sigma_{33,3} = -\mathbf{L}^{\mathrm{T}}\boldsymbol{\sigma}_s, \tag{17}$$

$$D_{3,3} = \mathbf{L}^{\mathrm{T}}(\boldsymbol{\kappa}\mathbf{L}\phi - d_s^{\mathrm{T}}\sigma_s), \tag{18}$$

$$\boldsymbol{\sigma}_p = \mathbf{S}_{pp}^{-1}(\mathbf{G}\mathbf{L}_p\mathbf{u} - \widetilde{\mathbf{S}}_{p3}\sigma_{33} - \widetilde{\kappa}_{33}^{-1}\mathbf{d}_pD_3), \tag{19}$$

$$\mathbf{D}_p = -\boldsymbol{\kappa}L\phi + \mathbf{d}_s^{\mathrm{T}}\boldsymbol{\sigma}_s, \tag{20}$$

where

$$\widetilde{\mathbf{S}}_{p3} = \mathbf{S}_{p3} - \widetilde{d}_{33}\mathbf{d}_p, \quad \widetilde{s}_{33} = s_{33} - \widetilde{d}_{33}d_{33}, \quad \mathbf{G} = \mathbf{I} + \widetilde{\kappa}_{33}^{-1}\mathbf{d}_p\mathbf{d}_p^{\mathrm{T}}\mathbf{S}_{pp}^{-1},$$

$$\widetilde{\kappa}_{33} = \kappa_{33} - \mathbf{d}_p^{\mathrm{T}}\mathbf{S}_{pp}^{-1}\mathbf{d}_p, \quad \widetilde{d}_{33} = \widetilde{\kappa}_{33}^{-1}(d_{33} - \mathbf{d}_p^{\mathrm{T}}\mathbf{S}_{pp}^{-1}\mathbf{S}_{p3}),$$

$$\mathbf{u} = \begin{bmatrix} u_1 \\ u_2 \end{bmatrix}, \quad \mathbf{L}_p^{\mathrm{T}} = \begin{bmatrix} \partial/\partial x_1 & 0 & \partial/\partial x_2 \\ 0 & \partial/\partial x_2 & \partial/\partial x_1 \end{bmatrix}.$$

The state equation for a linear piezoelectric material is obtained by arranging Eqs. (13)–(18) into a matrix differential equation. For problems of generalized plane strain in which the field variables are independent of x_2 the state equation becomes

$$\frac{\partial}{\partial x_3}\begin{bmatrix} u_1 \\ u_2 \\ u_3 \\ \phi \\ \sigma_{13} \\ \sigma_{23} \\ \sigma_{33} \\ D_3 \end{bmatrix} = \begin{bmatrix} 0 & 0 & -\partial_1 & l_{14} & s_{44} & s_{45} & 0 & 0 \\ 0 & 0 & 0 & l_{15} & s_{45} & s_{55} & 0 & 0 \\ l_{31} & l_{32} & 0 & 0 & 0 & 0 & a_{37} & \widetilde{d}_{33} \\ l_{41} & l_{42} & 0 & 0 & 0 & 0 & \widetilde{d}_{33} & -\widetilde{\kappa}_{33}^{-1} \\ l_{51} & l_{52} & 0 & 0 & 0 & 0 & l_{31} & l_{41} \\ l_{52} & l_{62} & 0 & 0 & 0 & 0 & l_{32} & l_{42} \\ 0 & 0 & 0 & 0 & -\partial_1 & 0 & 0 & 0 \\ 0 & 0 & 0 & l_{84} & l_{14} & l_{15} & 0 & 0 \end{bmatrix} \begin{bmatrix} u_1 \\ u_2 \\ u_3 \\ \phi \\ \sigma_{13} \\ \sigma_{23} \\ \sigma_{33} \\ D_3 \end{bmatrix}, \tag{21}$$

where

$$l_{14} = -d_{14}\partial_1, \quad l_{15} = -d_{15}\partial_1, \quad l_{31} = a_{31}\partial_1, \quad l_{32} = a_{32}\partial_1,$$

$$l_{41} = a_{41}\partial_1, \quad l_{42} = a_{42}\partial_1, \quad l_{51} = a_{51}\partial_{11}, \quad l_{52} = a_{52}\partial_{11}, \quad l_{62} = a_{62}\partial_{11},$$

$$l_{84} = \kappa_{11}\partial_{11}, \quad [\,a_{31} \quad a_{32}\,] = \widetilde{\mathbf{S}}_{p3}^{\mathrm{T}}\mathbf{S}_{pp}^{-1}\mathbf{H}^{\mathrm{T}}, \quad a_{37} = \widetilde{s}_{33} - \mathbf{S}_{p3}^{\mathrm{T}}\mathbf{S}_{pp}^{-1}\widetilde{\mathbf{S}}_{p3},$$

$$\begin{bmatrix} a_{41} \\ a_{42} \end{bmatrix} = \widetilde{\kappa}_{33}^{-1}\mathbf{H}\mathbf{S}_{pp}^{-1}\mathbf{d}_p, \quad \begin{bmatrix} a_{51} & a_{52} \\ a_{52} & a_{62} \end{bmatrix} = -\mathbf{H}\mathbf{S}_{pp}^{-1}\mathbf{G}\mathbf{H}^{\mathrm{T}}, \quad \mathbf{H} = \begin{bmatrix} 1 & 0 & 0 \\ 0 & 0 & 1 \end{bmatrix}.$$

The output Eqs. (19) and (20) are

$$\begin{bmatrix} \sigma_{11} \\ \sigma_{22} \\ \sigma_{12} \end{bmatrix} = \begin{bmatrix} b_{11} & b_{12} \\ b_{21} & b_{22} \\ b_{31} & b_{32} \end{bmatrix} \frac{\partial}{\partial x_1}\begin{bmatrix} u_1 \\ u_2 \end{bmatrix} + \begin{bmatrix} b_{17} \\ b_{27} \\ b_{37} \end{bmatrix}\sigma_{33} + \begin{bmatrix} b_{18} \\ b_{28} \\ b_{38} \end{bmatrix} D_3, \tag{22}$$

$$\begin{bmatrix} D_1 \\ D_2 \end{bmatrix} = -\begin{bmatrix} \kappa_{11} \\ \kappa_{12} \end{bmatrix}\phi_{,1} + \begin{bmatrix} d_{14} & d_{15} \\ d_{24} & d_{25} \end{bmatrix}\begin{bmatrix} \sigma_{13} \\ \sigma_{23} \end{bmatrix}, \tag{23}$$

where

$$\begin{bmatrix} b_{11} & b_{12} \\ b_{21} & b_{22} \\ b_{31} & b_{32} \end{bmatrix} = \mathbf{S}_{pp}^{-1}\mathbf{G}\mathbf{H}^{\mathrm{T}}, \quad \begin{bmatrix} b_{17} \\ b_{27} \\ b_{37} \end{bmatrix} = -\mathbf{S}_{pp}^{-1}\widetilde{\mathbf{S}}_{p3}, \quad \begin{bmatrix} b_{18} \\ b_{28} \\ b_{38} \end{bmatrix} = -\widetilde{\kappa}_{33}^{-1}\mathbf{S}_{pp}^{-1}\mathbf{d}_p.$$

It is understood that Eqs. (21)–(23) are applicable to each layer of the laminate; the subscript k has been dropped. Note that both the antiplane and inplane field variables appear in the formulation.

3. Eigensolution and decay rate

We seek the solution to Eq. (21) in the form

$$\begin{aligned}[u_1 \quad u_2 \quad u_3 \quad \phi \quad \sigma_{13} \quad \sigma_{23} \quad \sigma_{33} \quad D_3\,]_k = {} & \mathrm{e}^{-\lambda x_1}[\,u \quad v \quad w \quad \varphi \quad \tau_{13} \quad \tau_{23} \quad \tau_{33} \quad \Lambda_3\,]_k \\ & + \mathrm{e}^{\gamma(x_1-a)}\big[\,\widetilde{u} \quad \widetilde{v} \quad \widetilde{w} \quad \widetilde{\varphi} \quad \widetilde{\tau}_{13} \quad \widetilde{\tau}_{23} \quad \widetilde{\tau}_{33} \quad \widetilde{\Lambda}_3\,\big]_k,\end{aligned} \tag{24}$$

where λ and γ are the decay factors to be determined; $u, v, w, \ldots, \Lambda_3$ and $\widetilde{u}, \widetilde{v}, \widetilde{w}, \ldots, \widetilde{\Lambda}_3$ are unknown functions of x_3. The first exponential function depicts the decay from the end $x_1 = 0$ with a decay rate λ; the

second depicts the decay from the end $x_1 = a$ with a decay rate γ. As in isotropic elasticity (Timoshenko and Goodier, 1970) the decay rates λ and γ are real or in complex conjugate pairs and their superpositions give the stress fields of the self-equilibrium state. As x_1 increases, the influence of the first term decreases, whereas the influence of the second term increases. It will be shown shortly that the decay rates from both ends of the laminate are the same. For a semi-infinite strip, $a \to \infty$, the second term vanishes, only the decay from $x_1 = 0$ needs to be considered.

Substitution of Eq. (24) in Eq. (21) yields two sets of equations as follows:

$$\frac{\mathrm{d}}{\mathrm{d}x_3}\mathbf{X}_k = \lambda \mathbf{A}_k \mathbf{X}_k, \qquad \frac{\mathrm{d}}{\mathrm{d}x_3}\widetilde{\mathbf{X}}_k = -\gamma \mathbf{A}_k \widetilde{\mathbf{X}}_k, \tag{25}$$

where the elements of the coefficient matrix $\mathbf{A}_k$ are given in Appendix A, and

$$\mathbf{X}_k = [\,\lambda u \quad \lambda v \quad \lambda w \quad \lambda \varphi \quad \tau_{13} \quad \tau_{23} \quad \tau_{33} \quad \Lambda_3\,]_k^{\mathrm{T}},$$

$$\widetilde{\mathbf{X}}_k = [\,-\gamma \widetilde{u} \quad -\gamma \widetilde{v} \quad -\gamma \widetilde{w} \quad -\gamma \widetilde{\varphi} \quad \widetilde{\tau}_{13} \quad \widetilde{\tau}_{23} \quad \widetilde{\tau}_{33} \quad \widetilde{\Lambda}_3\,]_k^{\mathrm{T}}.$$

It is easily observed that Eqs. (25) and (26) are precisely the same if $\gamma = -\lambda$. This indicates that the decay rates from both ends are the same and both equations result in the same through-the-thickness variation of the field variables. Moreover, it tells us that if λ_i is a decay factor so is $-\lambda_i$. Consequently, we may treat either Eq. (25) first part or Eq. (25) second part. In the following we treat Eq. (25) first part. Note that we have arranged Eq. (25) in such a way that the coefficient matrices do not contain the decay factor. This makes the eigensolution by means of matrix algebra easier.

The solution of the first equation in Eq. (25) is

$$\mathbf{X}_k(x_3) = \mathbf{P}_k(x_3 - z_{k-1})\mathbf{X}_k(z_{k-1}), \tag{26}$$

where the fundamental transfer matrix (Pease, 1965) $\mathbf{P}_k$ is

$$\mathbf{P}_k(x_3 - z_{k-1}) = \mathrm{e}^{\lambda \mathbf{A}_k (x_3 - z_{k-1})}. \tag{27}$$

The interfacial continuity conditions are satisfied by letting

$$\mathbf{X}_{k+1}(z_k) = \mathbf{X}_k(z_k). \tag{28}$$

There follows

$$\mathbf{X}_{k+1}(z_k) = \mathbf{P}_k(z_k - z_{k-1})\mathbf{X}_k(z_{k-1}) \tag{29}$$

for $k = 1, 2, \ldots, n-1$.

Using Eq. (29) recursively yields

$$\mathbf{X}(x_3) = \mathbf{T}_k(x_3)\mathbf{X}(h), \quad z_{k-1} \leqslant x_3 \leqslant z_k \tag{30}$$

where

$$\mathbf{T}_k(x_3) = \begin{cases} \mathbf{P}_1(x_3 - h), & k = 1; \\ \mathbf{P}_k(x_3 - z_{k-1})\mathbf{T}_{k-1}(z_{k-1}), & k = 2, 3, \ldots, n. \end{cases} \tag{31}$$

Setting $x_3 = -h$ in Eq. (30) gives

$$\mathbf{X}(-h) = \mathbf{T}_n(-h)\mathbf{X}(h). \tag{32}$$

Consideration of the BC on $x_3 = \pm h$ is in order. To facilitate satisfaction of the BC, we partition Eq. (32) into

$$\begin{bmatrix} \mathbf{U}(-h) \\ \mathbf{S}(-h) \end{bmatrix} = \begin{bmatrix} \mathbf{T}_{uu}(-h) & \mathbf{T}_{us}(-h) \\ \mathbf{T}_{su}(-h) & \mathbf{T}_{ss}(-h) \end{bmatrix} \begin{bmatrix} \mathbf{U}(h) \\ \mathbf{S}(h) \end{bmatrix}, \tag{33}$$

where

$$\mathbf{U} = \lambda[\, u \quad v \quad w \quad \varphi\,]^{\mathrm{T}}, \quad \mathbf{S} = [\, \tau_{13} \quad \tau_{23} \quad \tau_{33} \quad \Lambda_3\,]^{\mathrm{T}}.$$

Let us consider first both the top and bottom surfaces are traction-free and electric-insulated. The boundary conditions demand $\mathbf{S}(h) = \mathbf{S}(-h) = 0$. It follows that

$$\mathbf{T}_{su}(-h)\mathbf{U}(h) = 0, \tag{34}$$

to which non-trivial $\mathbf{U}(h)$ exists if the determinant of the coefficient matrix vanishes,

$$|\mathbf{T}_{su}(-h)| = 0 \tag{35}$$

from which the decay factor λ, subsequently the $\mathbf{U}(h)$, can be determined.

The primary state variables are determined from

$$\mathbf{U}(x_3) = \mathbf{T}_{uu}(x_3)\mathbf{U}(h), \quad \mathbf{S}(x_3) = \mathbf{T}_{su}(x_3)\mathbf{U}(h). \tag{36}$$

When both the top and bottom surfaces are grounded, Eq. (32) is partitioned into

$$\begin{bmatrix} \widehat{\mathbf{U}}(-h) \\ \widehat{\mathbf{S}}(-h) \end{bmatrix} = \begin{bmatrix} \widehat{\mathbf{T}}_{uu}(-h) & \widehat{\mathbf{T}}_{us}(-h) \\ \widehat{\mathbf{T}}_{su}(-h) & \widehat{\mathbf{T}}_{ss}(-h) \end{bmatrix} \begin{bmatrix} \widehat{\mathbf{U}}(h) \\ \widehat{\mathbf{S}}(h) \end{bmatrix}, \tag{37}$$

where

$$\widehat{\mathbf{U}} = [\, \lambda u \quad \lambda v \quad \lambda w \quad \Lambda_3\,]^{\mathrm{T}}, \quad \widehat{\mathbf{S}} = [\, \tau_{13} \quad \tau_{23} \quad \tau_{33} \quad \lambda\varphi\,]^{\mathrm{T}}.$$

With the BC: $\widehat{\mathbf{S}}(h) = \widehat{\mathbf{S}}(-h) = 0$, the decay factor is determined from

$$|\widehat{\mathbf{T}}_{su}(-h)| = 0, \tag{38}$$

and the primary state variables from

$$\widehat{\mathbf{U}}(x_3) = \widehat{\mathbf{T}}_{uu}(x_3)\widehat{\mathbf{U}}(h), \quad \widehat{\mathbf{S}}(x_3) = \widehat{\mathbf{T}}_{su}(x_3)\widehat{\mathbf{U}}(h). \tag{39}$$

In a similar way, the decay factor and the internal field can be determined when one surface is electric-insulated and the other is grounded. Once the primary state variables are determined, the other stress and electric displacement components are

$$\begin{bmatrix} \sigma_{11} \\ \sigma_{22} \\ \sigma_{12} \end{bmatrix}_k = \mathrm{e}^{-\lambda x_1} \left(- \begin{bmatrix} b_{11} & b_{12} \\ b_{21} & b_{22} \\ b_{31} & b_{32} \end{bmatrix}_k \begin{bmatrix} \lambda u \\ \lambda v \end{bmatrix}_k + \begin{bmatrix} b_{17} \\ b_{27} \\ b_{37} \end{bmatrix}_k \tau_{33k} + \begin{bmatrix} b_{18} \\ b_{28} \\ b_{38} \end{bmatrix}_k \Lambda_{3k} \right), \tag{40}$$

$$\begin{bmatrix} D_1 \\ D_2 \end{bmatrix}_k = \mathrm{e}^{-\lambda x_1} \left(\begin{bmatrix} \kappa_{11} \\ \kappa_{12} \end{bmatrix}_k \lambda\varphi_k + \begin{bmatrix} d_{14} & d_{15} \\ d_{24} & d_{25} \end{bmatrix}_k \begin{bmatrix} \tau_{13} \\ \tau_{23} \end{bmatrix}_k \right). \tag{41}$$

This completes the determination of the decay factor and the eigen mode in a self-equilibrated piezoelectric laminate. To evaluate the coupling effects on the attenuation rate, let us follow Miller and Horgan (1995) by defining the *characteristic decay length* l as the length over which the field variables decay to 1% of their values at $x_1 = 0$,

$$l = \ln 100/\lambda. \tag{42}$$

The characteristic decay length is a measure of the distance from the end beyond which the end effect is negligible. The smallest decay factor should be used in Eq. (42) to evaluate the characteristic decay length.

4. Piezoelectric strips

Before computing the decay factor λ and the internal field for a given material, it is informative to examine the equations for a piezoelectric material of the *orthorhombic* system. Since the inplane and antiplane deformation and stresses are uncoupled in the state of generalized plane strain of an orthotropic elastic material (Lekhnitskii, 1981), one might presume that the antiplane field variables for generalized plane strain of an orthorhombic piezoelectric material are immaterial as well. This proves to be incorrect.

Obviously, all the 3-D electromechanical variables enter the stage and the inplane and antiplane field variables are coupled in a *monoclinic* piezoelectric strip. For piezoelectric materials of the orthorhombic system of class *mm*2, the first equation in Eq. (25) reduces to

$$\frac{\mathrm{d}}{\mathrm{d}x_3}\begin{bmatrix}\lambda u\\ \lambda w\\ \lambda\varphi\\ \tau_{13}\\ \tau_{33}\\ \Lambda_3\end{bmatrix}=\lambda\left(\begin{bmatrix}0 & 1 & 0 & s_{44} & 0 & 0\\ -a_{31} & 0 & 0 & 0 & a_{37} & \widetilde{d}_{33}\\ -a_{41} & 0 & 0 & 0 & \widetilde{d}_{33} & -\widetilde{\kappa}_{33}^{-1}\\ a_{51} & 0 & 0 & 0 & -a_{31} & -a_{41}\\ 0 & 0 & 0 & 1 & 0 & 0\\ 0 & 0 & \kappa_{11} & 0 & 0 & 0\end{bmatrix}\begin{bmatrix}\lambda u\\ \lambda w\\ \lambda\varphi\\ \tau_{13}\\ \tau_{33}\\ \Lambda_3\end{bmatrix}+\begin{bmatrix}0\\0\\0\\0\\0\\d_{15}\end{bmatrix}\tau_{23}\right), \tag{43}$$

$$\frac{\mathrm{d}}{\mathrm{d}x_3}\begin{bmatrix}\lambda v\\ \tau_{23}\end{bmatrix}=\lambda\left(\begin{bmatrix}0 & s_{55}\\ 1/s_{66} & 0\end{bmatrix}\begin{bmatrix}\lambda v\\ \tau_{23}\end{bmatrix}+\begin{bmatrix}d_{15}\\ 0\end{bmatrix}\lambda\varphi\right). \tag{44}$$

The output equations reduce to

$$\begin{bmatrix}\sigma_{11}\\ \sigma_{22}\end{bmatrix}=\frac{\mathrm{e}^{-\lambda x_1}}{\varkappa}\left(-\begin{bmatrix}b_{11}\\ b_{21}\end{bmatrix}\lambda u+\begin{bmatrix}b_{17}\\ b_{27}\end{bmatrix}\tau_{33}+\begin{bmatrix}b_{18}\\ b_{28}\end{bmatrix}\Lambda_3\right),\quad \sigma_{12}=-\frac{\mathrm{e}^{-\lambda x_1}}{s_{66}}\lambda v, \tag{45}$$

$$D_1=\mathrm{e}^{-\lambda x_1}(\kappa_{11}\lambda\varphi+d_{15}\tau_{23}),\quad D_2=\mathrm{e}^{-\lambda x_1}d_{24}\tau_{13}, \tag{46}$$

where

$$a_{31}=(\widetilde{s}_{13}s_{22}-\widetilde{s}_{23}s_{12})/\varkappa,\quad a_{41}=\widetilde{\kappa}_{33}^{-1}(d_{31}s_{22}-d_{32}s_{12})/\varkappa,$$

$$a_{37}=\widetilde{s}_{33}+[s_{23}(\widetilde{s}_{13}s_{12}-\widetilde{s}_{23}s_{11})-s_{13}(\widetilde{s}_{13}s_{22}-\widetilde{s}_{23}s_{12})]/\varkappa,$$

$$a_{51}=\widetilde{\kappa}_{33}^{-1}(d_{32}^2s_{12}^2-d_{31}^2s_{22}^2)/\varkappa^2-s_{22}/\varkappa,\quad \varkappa=s_{11}s_{22}-s_{12}^2,$$

$$\begin{bmatrix}b_{11}\\ b_{21}\end{bmatrix}=\begin{bmatrix}s_{22}+\widetilde{\kappa}_{33}^{-1}[s_{22}(d_{31}^2s_{22}-d_{31}d_{32}s_{12})+s_{12}(d_{32}^2s_{12}-d_{31}d_{32}s_{22})]/\varkappa\\ -s_{12}-\widetilde{\kappa}_{33}^{-1}[s_{11}(d_{32}^2s_{12}-d_{31}d_{32}s_{22})+s_{12}(d_{31}^2s_{22}-d_{31}d_{32}s_{12})]/\varkappa\end{bmatrix},$$

$$\begin{bmatrix}b_{17}\\ b_{27}\end{bmatrix}=\begin{bmatrix}\widetilde{s}_{23}s_{12}-\widetilde{s}_{13}s_{22}\\ \widetilde{s}_{13}s_{12}-\widetilde{s}_{23}s_{11}\end{bmatrix},\quad \begin{bmatrix}b_{18}\\ b_{28}\end{bmatrix}=\widetilde{\kappa}_{33}^{-1}\begin{bmatrix}d_{32}s_{12}-d_{31}s_{22}\\ d_{31}s_{12}-d_{32}s_{11}\end{bmatrix}.$$

It is evident from Eqs. (43) and (44) that the field variables in the x_1–x_3 plane are associated with the antiplane shear τ_{23}, and the antiplane deformation and shear stress are associated with the electromechanical field in the x_1–x_3 plane through φ. The inplane and antiplane field variables are coupled unless $d_{15}=0$. For the orthorhombic system of class 6*mm*. Eqs. (43)–(46) are somewhat simplified but the d_{15} remains in presence and these equations are still coupled. Only in orthorhombic piezoelectric materials with $d_{15}=0$ does a 2-D loading give rise to plane deformation and the antiplane shears σ_{12}, σ_{23} and displacement u_2 are independent of the electric field. From the material properties of various piezoelectric materials listed in Table 1 of Ruan et al. (2000), all of them have non-zero d_{15}. This suggests that the applicability of a 2-D

Table 1
Material constants of selected materials

	PZT-5	PVDF	Gr/Ep	Al
Elastic compliances (10^{-12} m^2/N)				
s_{11}	16.4	441	5.5	14.29
s_{12}	−5.74	−100	−1.5	−4.95
s_{13}	7.22	−304	−1.5	−4.95
s_{22}	16.4	504	97.1	14.29
s_{23}	7.22	−318	−32	−4.95
s_{33}	18.8	1134	97.1	14.29
s_{44}	47.5	1818	348.4	38.46
s_{55}	47.5	1695	139.5	38.46
s_{66}	44.28	1449	139.5	38.46
Piezoelectric constants (10^{-12} C/N)				
d_{15}	584	−27	0	0
d_{24}	584	−23	0	0
d_{31}	−172	21	0	0
d_{32}	−472	1.5	0	0
d_{33}	374	−32.5	0	0
d_{36}	0	0	0	0
Relative permittivities ($k_0 = 8.85 \times 10^{-12}$ F/m)				
k_{11}/k_0	1730	6.1	1730	1
k_{12}/k_0	0	0	0	0
k_{22}/k_0	1730	7.5	1730	1
k_{33}/k_0	1700	6.7	1730	1

formulation for piezoelectric strips without accounting for the antiplane field variables is very limited. The plane strain or plane stress assumption is invalid for electroelastic analysis in general.

To understand the Saint-Venant end effects in piezoelectric strips, we have computed the decay rate and characteristic decay length for a strip of a PZT ceramics, a PVDF polymer, and an aluminum (Al) metal. The material properties of PZT-5, PVDF, and Al used in the computation are given in Table 1. The stiffnesses of PZT-5, Gr/Ep, and Al are in the same order of magnitude, whereas the stiffness of PVDF is more than an order of magnitude smaller than that of Al, and the piezoelectric constants and permittivities of PZT-5 are more than an order of magnitude larger than those of PVDF. The constitutive equations for PZT and PVDF are similar to those for the orthorhombic system of class $6mm$, with $s_{16} = s_{26} = s_{36} = s_{45} = d_{14} = d_{25} = d_{36} = \kappa_{12} = 0$, $s_{11} = s_{22}$, $s_{13} = s_{23}$, $s_{44} = s_{55}$, $s_{66} = 2(s_{11} - s_{12})$, $d_{15} = d_{24}$, $d_{31} = d_{32}$, $\kappa_{11} = \kappa_{22}$. Note that d_{15} is non-zero, one cannot assume plane strain or plane stress and disregards the antiplane field variables. The numerical results show that antiplane shears and electric displacement D_2 indeed arise in orthorhombic piezoelectric strips and affect the decay behavior. Taking the PZT-5 strip for example, the first 10 decay rates and the characteristic decay length are given in Table 2, in which the results of Ruan et al. (2000) are listed for comparison. The reference length for the dimensionless decay rates is taken to be a half of the thickness as used in Ruan et al. The S and A in the table indicate the symmetric and the antisymmetric mode, respectively, The M denotes the decay rate associated with the mechanical mode. Note that all the decay rates due to antiplane modes are not obtainable and the characteristic decay lengths are greatly underestimated based on the plane strain assumption. The discrepancy between the decay lengths that account for and that neglect the antiplane deformation could be as much as 25%.

As stated before, the decay factor appears in pairs with the same magnitude of the positive and negative real parts. The positive ones correspond to decay from $x_1 = 0$ and the negative ones correspond to decay from the other end. In an Al strip there is no piezoelectric effect but electric conduction exists. In order to

Table 2
Stress decay in a PZT-5 layer, both surfaces grounded

Mode	Present	Ruan et al. (2000)
1	1.461	–
2	1.517 (M)	–
3	1.857 + i1.079 (S)	1.943 + i1.098 (S)
4	1.857 − i1.079 (S)	1.943 − i1.098 (S)
5	2.920	–
6	3.033 (M)	–
7	3.280 + i1.444 (A)	3.440 + i1.432 (A)
8	3.280 − i1.444 (A)	3.440 − i1.432 (A)
9	4.379	–
10	4.550 (M)	–
Decay length	$1.576 \times 2h$	$1.185 \times 2h$

M: mechanical mode, S: symmetric mode, A: antisymmetric mode.

distinguish whether the smallest decay rate is indeed associated with the stress decay rather than the decay of the electric field, we deliberately set $d_{ij} = 0$ and $k_{ij} = 0$ and $d_{ij} = 0$ and $k_{ij} \neq 0$ for a piezoelectric material to obtain hypothetical results that represent omitting of the piezoelectric effect completely ($d_{ij} = 0$, $k_{ij} = 0$) and omitting the piezoelastic coupling in particular ($d_{ij} = 0$, $k_{ij} \neq 0$). By comparing the actual results with the hypothetical ones, the modes that correspond to a *purely mechanical mode* (denoted by M), a *purely electric mode* (denoted by E), and a *coupling mode* (denoted by C) can be identified. We also examine the effects of the electric boundary conditions on $x_3 = \pm h$ on the decay by considering three types of the electric BC, namely, both surfaces insulated (case 1), both surfaces grounded (case 2), and insulated on $x_3 = -h$ and grounded on $x_3 = h$ (case 3).

Table 3 summarizes the results of the first five decay rates and the characteristic decay lengths, in which the reference length is taken to be the thickness of the strip as symmetry with respect to the midplane is not assumed. For Al the first mechanical mode is due to the antiplane deformation, the second one is due to the inplane deformation. The decay rates obtained agree with the exact solution (Timoshenko and Goodier, 1970; Wang et al., 2000). In PZT the characteristic decay lengths for the mechanical mode are $1.576 \times 2h$ (cases 1 and 2) and $3.153 \times 2h$ (case 3), in PVDF they are $1.642 \times 2h$ (all three cases). The three types of electric boundary conditions result in the same decay rate and decay length for the mechanical mode in PVDF and Al. In case the top surface is grounded and the bottom surface insulated, the decay length in PZT is twice that of both surfaces insulated or grounded. This suggests that the unsymmetrical BC prolongs the stress decay in materials with strong piezoelectric effects. Case 3 also yields the decay length twice those of the electric modes in Al, PVDF and PZT.

In the case of a homogeneous orthorhombic piezoelectric strip, the characteristic equation derived from Eq. (25) can be factorized as

$$(\mu^2 + k_{11}/k_{33})(\mu^2 + s_{44}/s_{66})\{\mu^4 + [c_{11}s_{55} - (2 + c_{13}s_{55})c_{13}/c_{33}]\mu^2 + c_{11}/c_{33}\} = 0, \tag{47}$$

where c_{ij} are elastic constants of the material, related to the elastic compliances by

$$c_{11} = (s_{22}s_{33} - s_{23}^2)/\Delta, \quad c_{13} = (s_{12}s_{23} - s_{13}s_{22})/\Delta, \quad c_{33} = (s_{21}s_{22} - s_{12}^2)/\Delta,$$
$$\Delta = s_{11}s_{22}s_{33} + 2s_{12}s_{23}s_{13} - s_{22}s_{13}^2 - s_{33}s_{13}^2 - s_{11}s_{23}^2.$$

The decay rates corresponding to the electric and mechanical modes can be evaluated analytically. The ones associated with

$$\mu^2 + k_{11}/k_{33} = 0 \tag{48}$$

Table 3
Decay rates and characteristic decay lengths for piezoelectric strips

Mode	Case 1	Case 2	Case 3
PZT-5			
1	2.921 (CS[a])	2.922 (CA[a])	1.461 (C)
2	3.033 (MA[b])	3.033 (MA[b])	3.033 (MA[b])
3	$3.714 \pm i2.158$ (CS[a])	$3.715 \pm i2.158$ (CS[a])	$3.715 \pm i2.158$ (C)
4	5.840 (CA[a])	5.841 (CS[a])	4.381 (C)
5	6.066 (MS[b])	6.066 (MS[b])	6.066 (MS[b])
Decay length	$1.576 \times 2h$ ($1.576 \times 2h$)	$1.576 \times 2h$ ($1.576 \times 2h$)	$3.153 \times 2h$ ($3.153 \times 2h$)
PVDF			
1	2.805 (MA[b])	2.805 (MA[b])	1.646 (E)
2	3.283 (CS[a])	$3.287 \pm i2.070$ (CS[a])	2.805 (MA[b])
3	$3.285 \pm i2.076$ (CS[a])	3.292 (EA[a])	$3.286 \pm i2.072$ (C[a])
4	5.610 (MS[b])	5.610 (MS[b])	4.923 (C)
5	6.543 (CA[a])	5.768 (CA[a])	5.610 (MS[b])
Decay length	$1.642 \times 2h$ ($1.403 \times 2h$)	$1.642 \times 2h$ ($1.401 \times 2h$)	$1.642 \times 2h$ ($2.798 \times 2h$)
Aluminum			
1	3.142 (EA[a])	3.142 (EA[a])	1.571 (E)
2	3.142 (MA[b])	3.142 (MA[b])	3.142 (MA[b])
3	$4.212 \pm i2.251$ (MS[a])	$4.212 \pm i2.251$ (MS[a])	$4.212 \pm i2.251$ (MS[a])
4	6.283 (ES[a])	6.283 (ES[a])	4.712 (E)
5	6.283 (MS[b])	6.283 (MS[b])	6.283 (MS[b])
Decay length	$1.466 \times 2h$ ($1.466 \times 2h$)	$1.466 \times 2h$ ($1.466 \times 2h$)	$1.466 \times 2h$ ($2.932 \times 2h$)

M: mechanical mode, E: electric mode, C: coupling mode, S: symmetric mode, A: antisymmetric mode.
[a] Inplane mode.
[b] Antiplane mode.

are purely electric modes, and the decay rates for the electric field are given by

$$\lambda = \begin{cases} n\pi(k_{33}/k_{11})^{1/2}, & \text{(cases 1 and 2)} \\ \frac{n\pi}{2}(k_{33}/k_{11})^{1/2}, & \text{(case 3)} \end{cases}, \tag{49}$$

where $n = 1, 2, \ldots$

The ones associated with

$$\mu^2 + s_{44}/s_{66} = 0 \tag{50}$$

are purely mechanical modes, and the decay rates are given by $\lambda = n\pi(s_{66}/s_{44})$, $n = 1, 2, \ldots$

The ones associated with

$$\mu^4 + [c_{11}s_{55} - (2 + c_{13}s_{55})c_{13}/c_{33}]\mu^2 + c_{11}/c_{33} = 0 \tag{51}$$

are also the mechanical modes.

As far as stress decay is concerned, the decay length should be evaluated using the smallest decay rate associated with a purely mechanical mode or a coupling mode. If the smallest one is associated with a purely electric mode, it corresponds to decay of the electric field. In Table 3 the underlined decay rates correspond to stress decay and were used in evaluating the characteristic decay length. The decay lengths given in the parenthesis correspond to decay of the electric field.

5. Piezoelectric laminates

As illustrations, we examine the Saint-Venant end effects in the active-sensory configuration in which piezoelectric layers are integrated on one face to act as the sensor and on the other as the actuator. A $[0/0/90]_s$ Gr/Ep composite laminate and an Al plate, both integrated with PZT and PVDF piezoelectric layers on the top and bottom surfaces, are considered. The material properties of the Gr/Ep lamina used in the computation are given in Table 1. Al and Gr/Ep are elastic materials with $d_{ij} = 0$. The electric BC on $x_3 = \pm h$ is assumed to be electric-insulated or grounded.

The decay rates and characteristic decay lengths for the $[0/0/90]_s$, $[\mathrm{PZT}/0/90]_s$, and $[\mathrm{PVDF}/0/90]_s$ laminated systems under three types of the electric conditions are shown in Table 4. The thickness of each layer is taken to be equal. It is interesting to observe that when the top and bottom layers of the Gr/Ep laminate are replaced by PZT layers, the characteristic decay lengths change from $2.849 \times 2h$ in all three cases to $2.775 \times 2h$ in cases 1 and 2, and $3.185 \times 2h$ in case 3. Since the stiffnesses of PZT ceramic and GR/Ep are comparable in magnitude, the changes are not very much. By contrast, when the top and bottom layers are replaced by PVDF layers, the characteristic decay lengths change drastically from $2.849 \times 2h$ to $1.543 \times 2h$ in all three cases. The large reduction is reasonable in that the stiffness of PVDF polymer is much lower than that of Gr/Ep. The soft PDVF layers act like energy absorbers in the system. To the opposite, if the laminate is bonded by stiff layers, the stress disturbance may extend to a long distance from the ends. In the extreme case of rigid layers, the disturbance affects the entire body.

Table 4
Decay rates and characteristic decay lengths for piezoelectric laminates

Mode	Case 1	Case 2	Case 3
[0/0/90]$_s$ Gr/Ep			
1	1.617 (MA[a])	1.617 (MA[a])	1.571 (E)
2	2.201 (MS[a])	2.201 (MS[a])	1.617 (MA[a])
3	2.470 (MA[b])	2.470 (MA[b])	2.201 (MS[a])
4	3.142 (EA[a])	3.142 (EA[a])	2.470 (MA[b])
5	3.793 (MS[a])	3.793 (MS[a])	3.793 (MS[a])
Decay length	$2.849 \times 2h$ ($1.466 \times 2h$)	$2.849 \times 2h$ ($1.466 \times 2h$)	$2.849 \times 2h$ ($2.932 \times 2h$)
[PZT/0/90]$_s$			
1	1.660 (MA[b])	1.660 (MA[b])	1.446 (C)
2	1.899 (CA[a])	1.886 (CA[a])	1.660 (MA[b])
3	2.836 (CS[a])	2.984 (CA[a])	1.907 (C)
4	$3.228 \pm i1.473$ (CS[a])	$3.103 \pm i1.500$ (CS[a])	$3.139 \pm i1.484$ (C)
5	3.751 (MS[b])	3.751 (MS[b])	3.751 (MS[b])
Decay length	$2.775 \times 2h$ ($2.425 \times 2h$)	$2.775 \times 2h$ ($2.442 \times 2h$)	$3.185 \times 2h$ ($3.185 \times 2h$)
[PVDF/0/90]$_s$			
1	2.990 (MA[a])	0.261 (EA[a])	0.185 (E)
2	3.843 (MA[b])	2.990 (MA[a])	2.990 (MA[a])
3	$4.468 \pm i1.590$ (MS[a])	3.843 (MA[b])	3.843 (MA[b])
4	4.563 (CS[a])	$4.467 \pm i1.595$ (MS[a])	$4.468 \pm i1.593$ (MS[a])
5	4.656 (CA[a])	4.602 (CS[a])	4.581 (C)
Decay length	$1.543 \times 2h$ ($1.009 \times 2h$)	$1.543 \times 2h$ ($17.619 \times 2h$)	$1.543 \times 2h$ ($24.959 \times 2h$)

M: mechanical mode, E: electric mode, C: coupling mode, S: symmetric mode, A: antisymmetric mode.
[a] Inplane mode.
[b] Antiplane mode.

Table 5
Decay rates and characteristic decay lengths for Al with piezoelectric layers

Mode	Case 1	Case 2	Case 3
[PZT/Al/PZT]			
1	0.160 (ES[a])	3.183 (MA[b])	0.113 (E)
2	3.183 (MA[b])	3.490 (EA[a])	3.183 (MA[b])
3	3.500 (EA[a])	$4.149 \pm i2.205$ (MS[a])	3.494 (E)
4	$4.149 \pm i2.209$ (MS[a])	6.361 (MS[b])	$4.149 \pm i2.207$ (C)
5	6.361 (MS[b])	6.981 (CS[a])	6.361 (MS[b])
Decay length	$1.447 \times 2h$ ($28.760 \times 2h$)	$1.447 \times 2h$ ($1.320 \times 2h$)	$1.447 \times 2h$ ($40.705 \times 2h$)
[PVDF/Al/PVDF]			
1	2.182 (ES[a])	3.432 (EA[a])	1.311 (E)
2	3.480 (MA[b])	3.480 (MA[b])	3.480 (MA[b])
3	$4.659 \pm i2.492$ (MS[a])	$4.659 \pm i2.492$ (MS[a])	4.185 (E)
4	4.802 (EA[a])	6.861 (ES[a])	$4.659 \pm i2.492$ (MS[a])
5	6.960 (MS[b])	6.960 (MS[b])	6.960 (MS[b])
Decay length	$1.323 \times 2h$ ($2.111 \times 2h$)	$1.323 \times 2h$ ($1.342 \times 2h$)	$1.323 \times 2h$ ($3.512 \times 2h$)

M: mechanical mode, E: electric mode, C: coupling mode, S: symmetric mode, A: antisymmetric mode.
[a] Inplane mode.
[b] Antiplane mode.

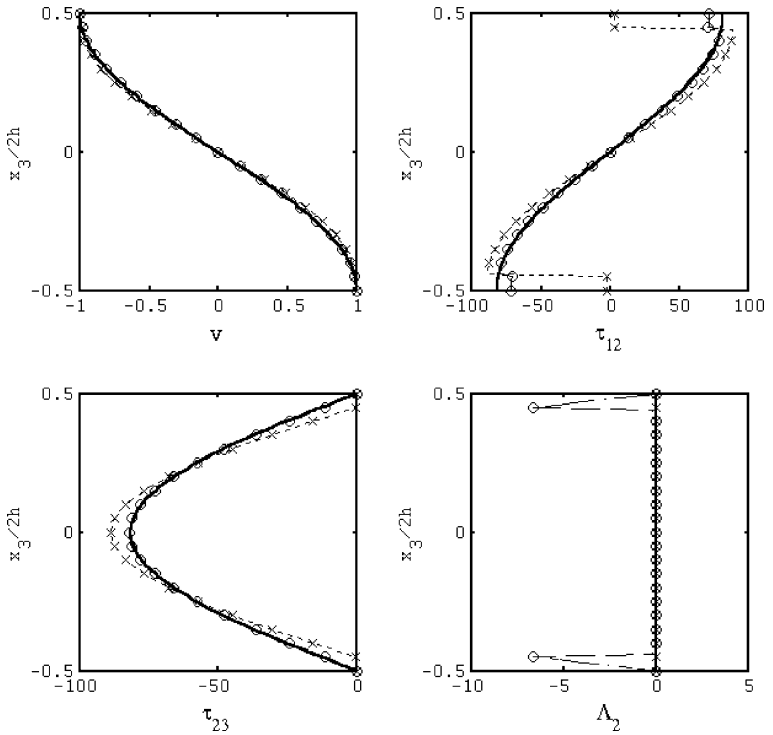

Fig. 2. Through-thickness variation of the first mechanical mode, antiplane deformation (Al: (—); PZT/Al/PZT: (- -○- -); PVDF/Al/PVDF: (· · × · ·)).

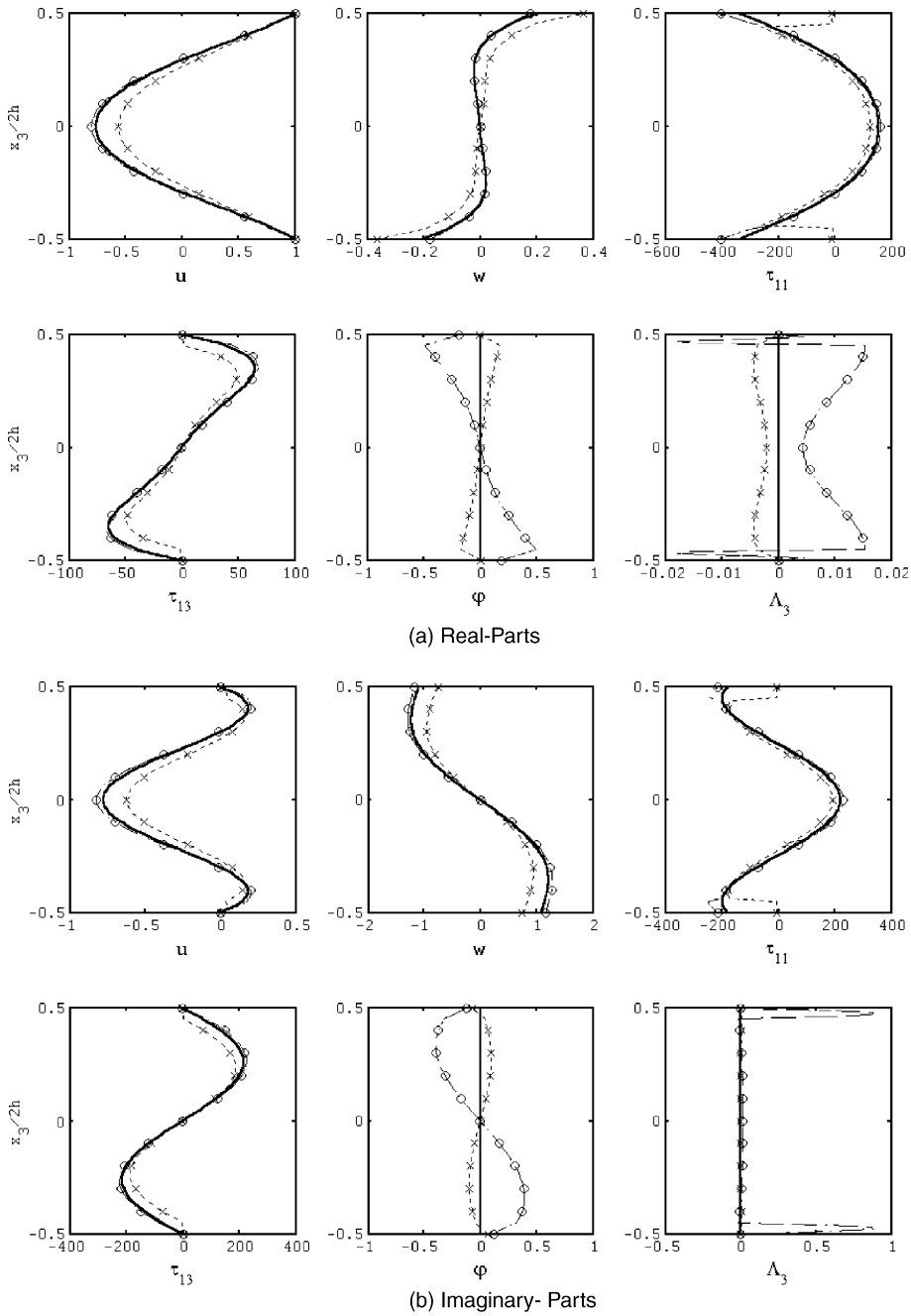

Fig. 3. Through-thickness variation of the second mechanical mode, inplane deformation (Al: (—); PZT/Al/PZT: (- -○- -); PVDF/Al/PVDF: (· · × · ·)).

Table 5 shows the decay rates and decay lengths for a homogeneous Al strip, and Al integrated with PZT and PVDF piezoelectric layers on the top and bottom surfaces. The thickness of the layers is taken to be

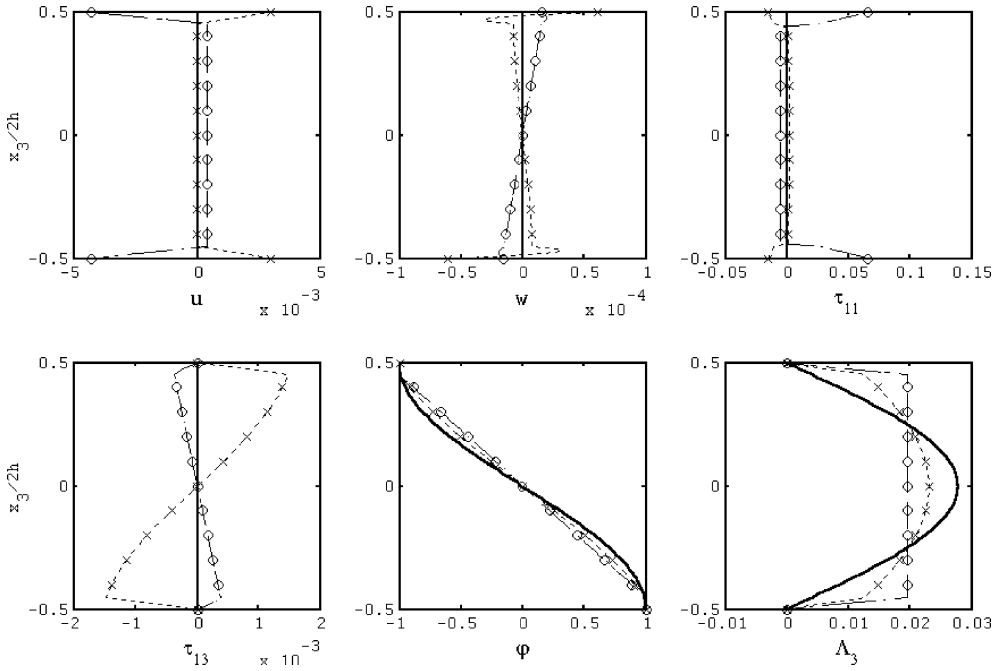

Fig. 4. Through-thickness variation of the first electric mode, case 1 (Al: (—); PZT/Al/PZT: (- -o- -); PVDF/Al/PVDF: (· · × · ·)).

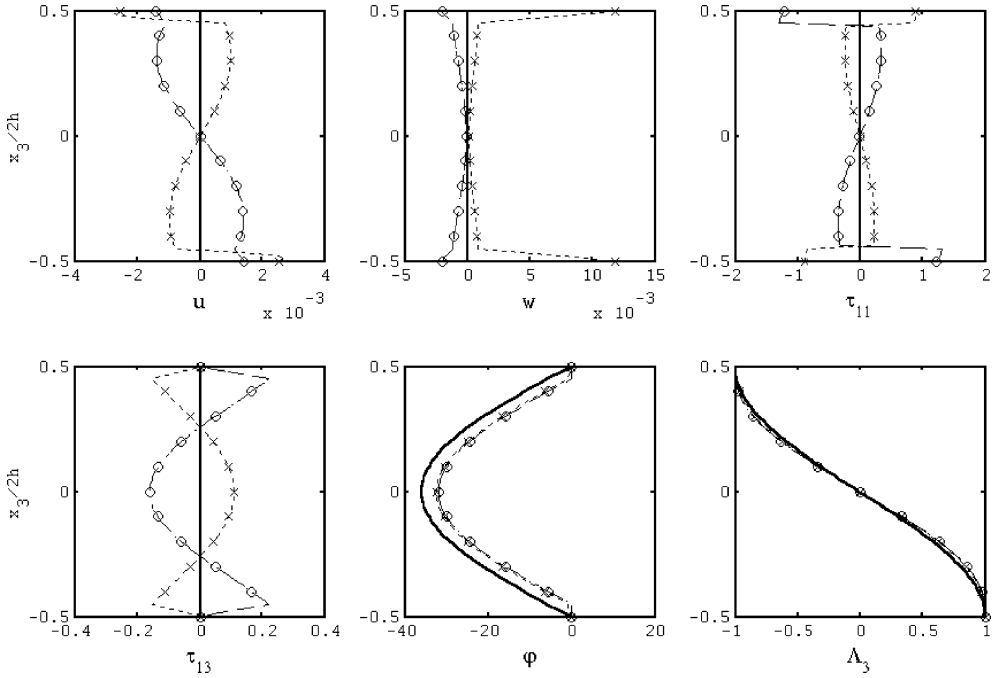

Fig. 5. Through-thickness variation of the first electric mode, case 2 (Al: (—); PZT/Al/PZT: (- -o- -); PVDF/Al/PVDF: (· · × · ·)).

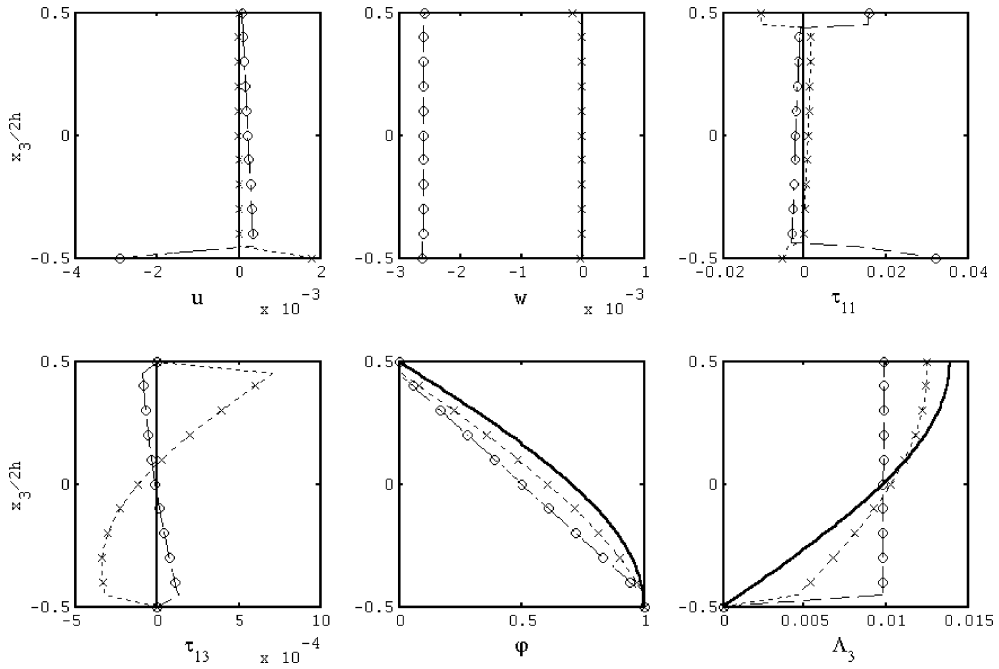

Fig. 6. Through-thickness variation of the first electric mode, case 3 (Al: (—); PZT/Al/PZT: (- -o- -); PVDF/Al/PVDF: (· · × · ·)).

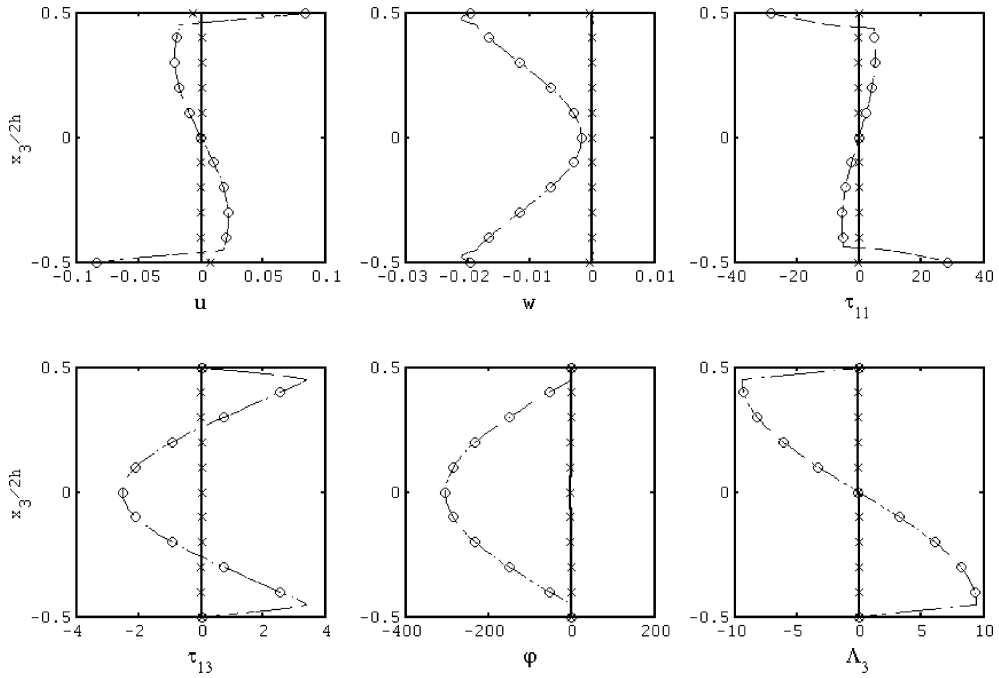

Fig. 7. Through-thickness variation of the second electric mode, case 1 (Al: (—); PZT/Al/PZT: (- -o- -); PVDF/Al/PVDF: (· · × · ·)).

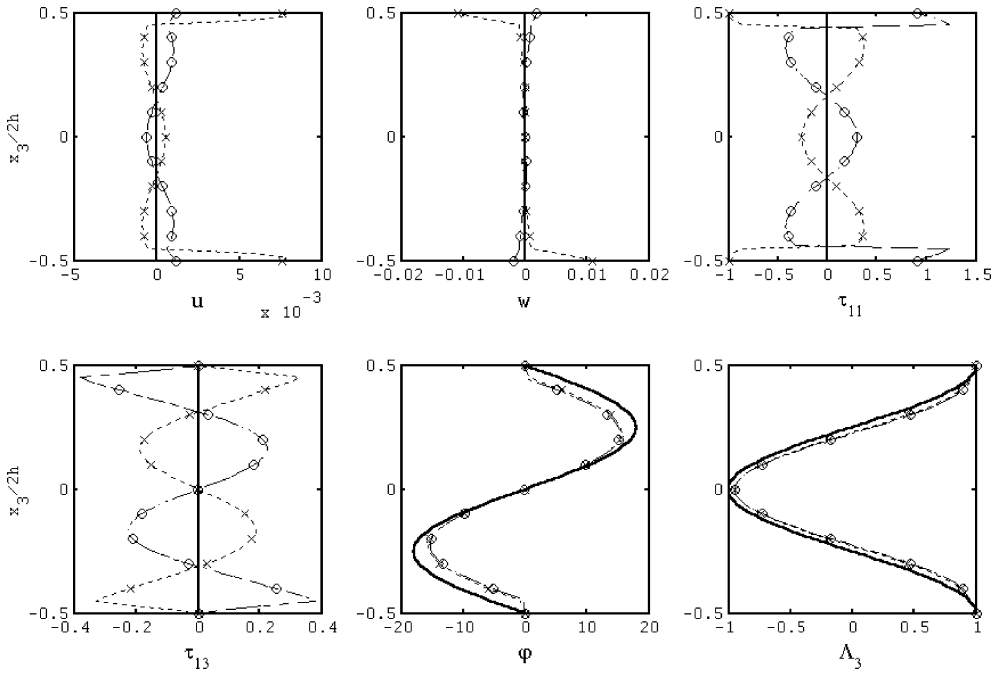

Fig. 8. Through-thickness variation of the second electric mode, case 2 (Al: (—); PZT/Al/PZT: (- -o- -); PVDF/Al/PVDF: (· · × · ·)).

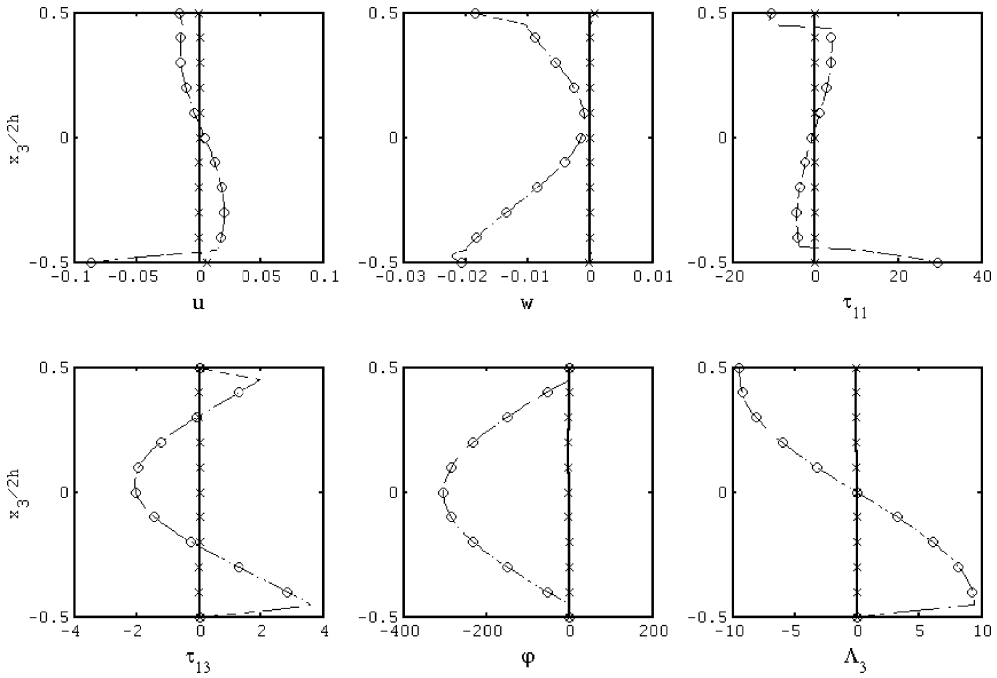

Fig. 9. Through-thickness variation of the second electric mode, case 3 (Al: (—); PZT/Al/PZT: (- -o- -); PVDF/Al/PVDF: (· · × · ·)).

$0.1h/1.8h/0.1h$. As compared with the results in Table 3, the characteristic decay lengths change from $1.466 \times 2h$ for a homogeneous Al strip to $1.323 \times 2h$ for the [PVDF/Al/PVDF] system and to $1.447 \times 2h$ for the [PZT/Al/PZT] system. The decay length reduces somewhat due to integrating the PVDF and PZT layers; a larger reduction is observed in the [PVDF/Al/PVDF] system. As for the decay length for the electric field, due to the low permittivity and zero piezoelectric constants of Al, it increases considerably, for example, it could change from $1.466 \times 2h$ (cases 1 and 2) and $2.932 \times 2h$ (case 3) in the homogeneous Al strip (see Table 3 for the electric mode) to $28.760 \times 2h$ (cases 1 and 2) and $42.705 \times 2h$ (case 3) in the [PZT/Al/PZT] system to reach a self-equilibrated electrostatic state.

To illustrate the piezoelectric effects and show the influence of the electric boundary conditions on the internal fields, we plot in Figs. 2–9 the through-thickness variations of the primary state variables at the edge $x_1 = 0$ of the homogeneous Al and the [PVDF/Al/PVDF] and [PZT/Al/PZT] systems under three types of the electric boundary conditions. As Al is elastic, the piezoelectric effects can be clearly observed by comparing the internal fields in the Al, with and without integrating the piezoelectric layers. Fig. 2 shows the through-thickness variation of the first mechanical mode due to the antiplane deformation. All the inplane variables are absent. The effects of piezoelectric coupling lead to non-zero electric displacement in the PZT layers. The field variables in the Al layer of the three systems under three types of the electric boundary conditions are almost the same. Fig. 3 shows the through-thickness variation of the first mechanical mode due to the inplane deformation. The mode consists of a real part and an imaginary part. All the antiplane variables are absent. The mechanical and the electric fields do not interact in the homogeneous Al layer. Since the through-thickness variations of the field variables under three types of the electric boundary conditions are alike (except for the transverse electric displacement), only the case of insulated surfaces (case 1) is presented. To show the piezoelectric effects on the electric field, we plot in Figs. 4–6 the first electric mode for case 1, case 2 and case 3. Again, the electric and the mechanical fields do not interact in the homogeneous Al layer. As a result of introducing the piezoelectric layers in the system, changes of the electromechanical fields in the Al, albeit small (in the order of 10^{-3} to 10^{-4}), arise because of the interfacial continuity. Marked changes of the internal field from that of the homogeneous Al occur in the second mode, as shown in Figs. 7–9. Changes in the displacement and stress in the Al due to integrating the PVDF layers on the surfaces are negligible, but they are significant due to integrating the PZT layers. In all cases the electric boundary conditions greatly affect the electric field through the thickness, but the displacement and stress fields in the Al of the three systems do not differ appreciably under different electric boundary conditions. The observations confirm the expectation that the mechanical field in a non-piezoelectric material should not be significantly affected by integrating a thin, weak piezoelectric layer on the surfaces. Thus, in dealing with the mechanical responses of the laminate with piezoelectric layers, it is reasonable to neglect the contribution of the stiffness of the weak piezoelectric layers on the surface for simplification, but the contribution of the stiff piezoelectric layers cannot be ignored. The electric field depends heavily on the electric boundary conditions, an assumed through-thickness distribution of the electric potential may lead to serious errors in evaluating the electromechanical field in the body.

6. Conclusions

The study provides an analytic solution for the stress decay in 2-D multilayered piezoelectric strips and laminates. The decay rates and the characteristic decay lengths in homogeneous strips and composite laminates have been evaluated for typical piezoelectric materials in the context of generalized plane strain. It has been shown that the formulation based on the plane strain or plane stress assumption is invalid except for a very special class of the orthorhombic piezoelectric material. The inplane field is coupled to the antiplane field which cannot be ignored in general even though the piezoelectric strip or laminate is subjected to a 2-D electromechanical loading. In evaluating the decay length in a piezoelectric material, at-

tention must be paid to distinguishing various modes lest the smallest eigenvalue should correspond to decay of the electric field rather than stress decay. The analysis shows that the electromechanical interaction has significant effects on the internal field in a self-equilibrated strip or laminate. The Saint-Venant end effects are more pronounced and the decay length far-reaching in homogeneous strips or composite laminates with stiff piezoelectric layers than with soft piezoelectric layers.

Acknowledgements

We thank Dr Y. M. Wang for helpful discussion. The work is supported by the National Science Council of Taiwan, ROC through grant NSC 90-2211-E006-060 and by National Cheng Kung University through a research fund.

Appendix A

The material matrices in Eq. (1) are

$$\mathbf{S}=\begin{bmatrix} s_{11} & s_{12} & s_{13} & 0 & 0 & s_{16} \\ s_{12} & s_{22} & s_{23} & 0 & 0 & s_{26} \\ s_{13} & s_{23} & s_{33} & 0 & 0 & s_{36} \\ 0 & 0 & 0 & s_{44} & s_{45} & 0 \\ 0 & 0 & 0 & s_{45} & s_{55} & 0 \\ s_{16} & s_{26} & s_{36} & 0 & 0 & s_{66} \end{bmatrix}, \quad \mathbf{d}=\begin{bmatrix} 0 & 0 & d_{31} \\ 0 & 0 & d_{32} \\ 0 & 0 & d_{33} \\ d_{14} & d_{24} & 0 \\ d_{15} & d_{25} & 0 \\ 0 & 0 & d_{36} \end{bmatrix}, \quad \boldsymbol{\kappa}=\begin{bmatrix} \kappa_{11} & \kappa_{12} & 0 \\ \kappa_{12} & \kappa_{22} & 0 \\ 0 & 0 & \kappa_{33} \end{bmatrix}.$$

The coefficient matrix in Eq. (25) is

$$\mathbf{A}_k=\begin{bmatrix} 0 & 0 & 1 & d_{14} & s_{44} & s_{45} & 0 & 0 \\ 0 & 0 & 0 & d_{15} & s_{45} & s_{55} & 0 & 0 \\ -a_{31} & -a_{32} & 0 & 0 & 0 & 0 & a_{37} & \widetilde{d}_{33} \\ -a_{41} & -a_{42} & 0 & 0 & 0 & 0 & \widetilde{d}_{33} & -\widetilde{\kappa}_{33}^{-1} \\ a_{51} & a_{52} & 0 & 0 & 0 & 0 & -a_{31} & -a_{41} \\ a_{52} & a_{62} & 0 & 0 & 0 & 0 & -a_{32} & -a_{42} \\ 0 & 0 & 0 & 0 & 1 & 0 & 0 & 0 \\ 0 & 0 & 0 & \kappa_{11} & d_{14} & d_{15} & 0 & 0 \end{bmatrix}_k.$$

References

Batra, R.C., Yang, J.S., 1995. Saint-Venant's principle in linear piezoelectricity. Journal of Elasticity 38, 209–218.

Gopinathan, S.V., Varadan, V., Varadan, V.K., 2000. Review and critique of theories for piezoelectric laminates. Smart Materials and Structures 9, 24–48.

Horgan, C.O., Knowles, J.K., 1983. Recent developments concerning Saint-Venant's principle. In: Hutchinson, J.W., Wu, T.Y., (Eds.), Advances in Applied Mechanics, vol. 23. Academic Press, New York, pp. 179–269.

Horgan, C.O., 1989. Recent developments concerning Saint-Venant's principle: an update. Applied Mechanics Review 42, 295–303.

Horgan, C.O., 1996. Recent developments concerning Saint-Venant's principle: a second update. Applied Mechanics Review 49, S101–S111.

Lekhnitskii, S.G., 1981. Theory of Elasticity of an Anisotropic Body. Mir, Moscow.

Miller, K.L., Horgan, C.O., 1995. Saint-Venant end effects for plane deformations of elastic composites. Mechanics of Composite Materials and Structures 2, 203–214.

Pease, M.C., 1965. Methods of Matrix Algebra. Academic Press, New York.

Nye, J.F., 1957. Physical Properties of Crystals. Oxford University Press, Oxford.

Ruan, X., Danforth, S.C., Safari, A., Chou, T.W., 2000. Saint-Venant end effects in piezoceramic materials. International Journal of Solids and Structures 37, 2625–2637.

Saravanos, D.A., Heyliger, P.R., 1999. Mechanics and computational models for laminated piezoelectric beams, plate, and shells. Applied Mechanics Review 52, 305–320.

Tarn, J.Q., 2001. Exact solutions for electroelastic analysis of generalized plane strain and torsion of piezoelectric cylinders. Chinese Journal of Mechanics 17, 149–156.

Tarn, J.Q., 2002a. Exact solutions of a piezoelectric circular tube or bar under extension, torsion, pressuring, shearing, uniform electric loading and temperature change. Proceeding of the Royal Soceity of London A, in press.

Tarn, J.Q., 2002b. A state space formalism for piezothermoelasticity. International Journal of Solids and Structure, in press.

Tarn, J.Q., Wang, Y.M., 2001. Laminated composite tubes under extension, torsion, bending, shearing and pressuring: a state space approach. International Journal of Solids and Structures 38, 9053–9075.

Tiersten, H.F., 1969. Linear Piezoelectric Plate Vibrations. Plenum Press, New York.

Timoshenko, S.P., Goodier, J.N., 1970. Theory of Elasticity, third ed. McGraw-Hill, New York.

Ting, T.C.T., 1996. Anisotropic Elasticity: Theory and Applications. Oxford University Press, Oxford.

Toupin, R.A., 1965. Saint-Venant's principle. Archives of Rational Mechanical Analysis 18, 83–96.

Wang, Y.M., Tarn, J.Q., Hsu, C.K., 2000. State space approach for stress decay in laminates. International Journal of Solids and Structures 37, 3535–3553.